A modelling study on ^{137}Cs and ^{239,240}Pu behaviour in the Alborán Sea, western Mediterranean

R. Periáñez*

Departamento Física Aplicada I, E.U. Ingeniería Técnica Agrícola, Universidad de Sevilla, Ctra., Utrera km 1, 41013 Sevilla, Spain

Abstract

A model for simulating the dispersion processes of ^{137}Cs and ^{239,240}Pu in the Alborán Sea is described. The model consists of two hydrodynamic models: a 2D depth-averaged model and a two-layer model which provide tidal and geostrophic currents, respectively; a sediment transport model which provides suspended particle concentrations and sedimentation rates over the domain; and the radionuclide dispersion model including interactions of dissolved radionuclides with suspended particles and bed sediments. These processes are formulated using kinetic transfer coefficients. The hydrodynamic and sediment models are run and validated in advance, and their results are then used to simulate the dispersion of ^{137}Cs and ^{239,240}Pu, which are introduced from atmospheric fallout. Radionuclide concentrations in the water column and distributions in bed sediments have been compared with measurements in the sea. Both set of data are, in general, in agreement. The model has also been applied to calculate radionuclide fluxes through the Strait of Gibraltar. These computed fluxes have been compared with previous estimations as well.

Keywords: Alborán Sea; Strait of Gibraltar; Numerical modelling; Dispersion; Hydrodynamics; Caesium; Plutonium

1. Introduction

The area of the Strait of Gibraltar and the Alborán Sea (Fig. 1) has a high ecological and economic value as the only connection between the Mediterranean Sea and the Atlantic Ocean. Moreover, the Alborán Sea is one of the most productive areas in the Mediterranean Sea (Masqué et al., 2003).

The basic circulation in the Strait of Gibraltar consists of an upper layer of fresher Atlantic water flowing into the Mediterranean Sea and an opposite deep current of denser Mediterranean water. The Atlantic inflow is slightly higher than the Mediterranean outflow to balance the excess of evaporation over river supply and precipitation in the Mediterranean Sea. The water exchanges through the Strait of Gibraltar have an influence in the biogeochemistry of the entire Mediterranean Sea. Substances with higher concentrations in deep water (nutrient profile) present a net loss through the Strait, experiencing a dilution in the Mediterranean. Thus, a negative budget for nutrients at the Strait of Gibraltar is determined. On the other hand, substances with higher concentrations in the surface waters of the

* Fax: +34 954486436.
E-mail address: rperianez@us.es

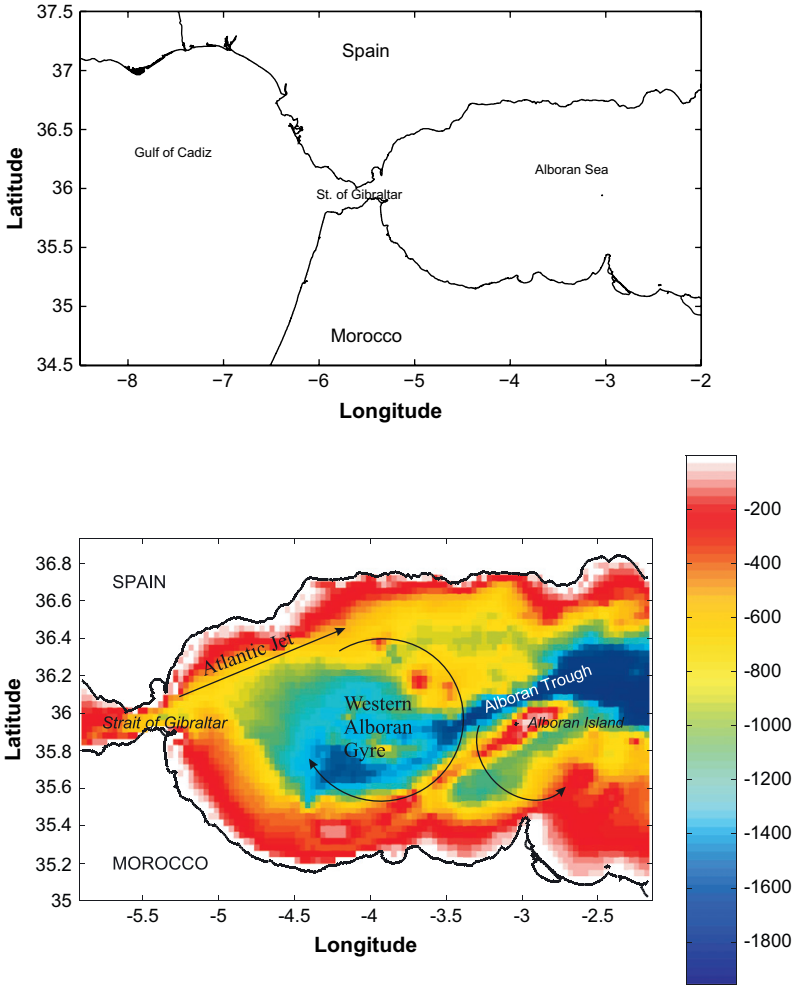

Fig. 1. General localization of the study area and topography of the Alborán Sea. Arrows indicate the general surface circulation pattern.

Gulf of Cádiz will be concentrated in an evaporative basin as the Mediterranean Sea. A considerable effort has been made in recent years to determine the budget of elements and radionuclides in the western Mediterranean and their fluxes through the Strait of Gibraltar (Van Geen and Boyle, 1990; Gómez, 2003; Gascó et al., 2002a; León-Vintró et al., 1999; Elbaz-Poulichet et al., 2001).

The objective of this work consists of studying, by means of numerical models, radionuclide dispersion and dynamics in the Alborán Sea. Some excellent works have already been published, which describe water circulation models for the area. Due to the particular dynamics of the Alborán Sea they are reduced-gravity or two-layer models (Preller, 1986; Werner et al., 1988; Heburn and La Violette, 1990; Castro-Díaz et al., 1994). Nevertheless, only a particle-tracking rapid-response dispersion model for dissolved radionuclides has been described for the region (Periáñez, 2006). Water circulation was obtained from a reduced-gravity model, thus only the dispersion of radionuclides released in the surface could be simulated. Consequently, interactions of radionuclides with sediments were neglected in such study. In this work, these processes are taken into account, thus sediment dynamics must be described as well.

Two different hydrodynamic models are applied to describe water circulation in the present work. A depth-averaged model is used to calculate tides and a two-layer model is used to obtain the residual (mean) flow. As will be shown, these are reasonable approaches. Of course, although a full 3D model could be used, we preferred the simplest approach that may be reasonably applied. The sediment transport model consists of an advection/diffusion equation to which some terms are added: settling, deposition, erosion, diffusion through the pycnocline and external

sources of particles. The radionuclide dispersion model also consists of an advection/diffusion equations with terms describing uptake/release reactions. This is done by means of kinetic transfer coefficients.

The dispersion model has been applied to two radionuclides: ^{137}Cs and ^{239,240}Pu. The major source of the anthropogenic radionuclides ^{137}Cs and ^{239,240}Pu has been the atmospheric deposition due to nuclear weapon tests, as well as the Chernobyl accident fallout in the case of ^{137}Cs. Other sources as discharges from nuclear facilities, riverine contributions and run-off from land may be neglected in the area (Gascó et al., 2002a).

Tides, residual flow, sedimentation rates (SR) and radionuclide distributions (in the water column and in the bed sediment) provided by the models have been compared with observations in the area. Radionuclide fluxes through the Strait of Gibraltar are also evaluated and compared with previous estimates. In general, there is a good agreement between model results and measurements. This is the first time, to the author knowledge, that a combination of depth-averaged and two-layer models is applied to simulate radionuclide dispersion in the marine environment. Moreover, this is the first time that these processes are studied in the Alborán Sea by means of numerical modelling.

A general description of the Alborán Sea is given in Section 2. Next, models are described: hydrodynamic, sediment transport and radionuclide dispersion models. Results are presented and discussed in Section 4. Finally, some of the sensitivity tests that have been carried out are presented (Section 4.4).

2. The Alborán Sea

The water circulation in the Strait of Gibraltar is characterized by a surface inflow (directed to the east) of Atlantic water and a deep outflow of more dense Mediterranean water (to the west). Exchanged flows are (Tsimplis and Bryden, 2000) of the order of 1 sverdrup (1 sverdrup $= 10^6$ m^3/s) with a net inflow into the Mediterranean Sea of about 0.05 sverdrup. This net inflow compensates the excess of evaporation over precipitation and river supply in the Mediterranean. A review on transport estimations through the Strait of Gibraltar may be seen in Bryden et al. (1994): from the very first carried out in 1877 and the widely cited value of 1.2 sverdrup for both outflow and inflow (Lacombe and Richez, 1982), to their own estimations of 0.72 and 0.68 sverdrup for inflow and outflow, respectively.

The water masses that may identified in the Alborán Sea are the Surface Atlantic Water (SAW) that has its origin in the North Atlantic Central Water (NACW) that has been modified by air−sea interactions, thus strictly speaking is not a water mass (Criado-Aldeanueva et al., 2006); the Surface Mediterranean Water (SMW) which occupies the surface layer in areas not reached by the SAW; the Levantine Intermediate Water (LIW) that flows from the Mediterranean to the Atlantic at depths between some 200 and 600 m and, finally, the Western Mediterranean Deep Water (WMDW), below the LIW and also flowing towards the Atlantic. However, this description may be simplified to a two-layer system with water flowing in opposite directions (Gascard and Richez, 1985; Farmer and Armi, 1988; Echevarría et al., 2002). Thus, from an operative point of view, SAW and SMW constitute the upper layer, and LIW and WMDW constitute the bottom layer, flowing to the west. Indeed, a steady westward flow of LIW and WMDW has been recorded in several experiments (Gascard and Richez, 1985; Parrilla et al., 1986). This approach has already been used to study the water exchanges between the Atlantic and the Mediterranean by means of numerical models (Izquierdo et al., 2001; Castro-Díaz et al., 1994; Preller, 1986; Heburn and La Violette, 1990).

The surface circulation in the Alborán Sea is represented in Fig. 1. The inflowing SAW penetrates the Strait of Gibraltar (see Fig. 2 for geographic names) and reaches mean velocities of the order of 0.6 m/s. This water forms a jet that enters the Alborán Sea in a east−northeast direction. The jet flows along the Spanish coast and curves to the south at about -3.5° longitude. Then part of it flows to the west, incorporating to an anticyclonic gyre, while the remainder flows to the African coast between Cape Tres Forcas and Alborán Isle (Perkins et al., 1990). The anticyclonic gyre is known as the Western Alborán Gyre (WAG). Another gyre, more elusive, fills the eastern basin of the Alborán Sea: it is the Eastern Alborán Gyre (EAG), that is out of the domain of our model. A detailed description may be seen for instance in Vargas-Yáñez et al. (2002), Vélez-Belchí et al. (2005) and references cited in these papers, which include the classical works carried out since the 1970s. The WAG is an almost permanent feature, although presents variations in intensity and even there are periods in which disappears (Vargas-Yáñez et al., 2002). The spatial scale of the WAG is about 100 km in diameter and some 200 m in depth.

Bryden and Stommel (1982) have found that the outflow of water from the Mediterranean to the Atlantic occurs along the Moroccan continental slope, and that this circulation appears to be nearly permanent feature of the southern side of the Alborán Sea.

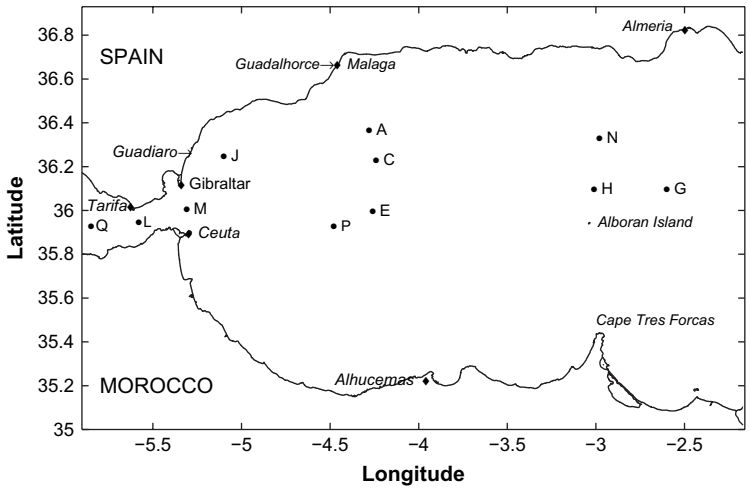

Fig. 2. Map of the Alborán Sea showing position of sampling points and geographical sites mentioned in the text. The two main rivers discharging in the area, Guadiaro and Guadalhorce, are also shown. Letters indicate points where computed radionuclide concentrations have been compared with observations.

With respect to the tides in the area, an important feature of the tidal flow in the Strait is that it can be considered, as a first approach, as barotropic. Indeed, 93% of the variance of current velocity in the semidiurnal band has a barotropic character in the Strait (Mañanes et al., 1998). Tsimplis and Bryden (2000) have pointed out that tidal currents are barotropic and larger than the mean inflow or outflow. The semidiurnal tide dominates current profile records in the Strait, obscuring the expected two-layer character of the mean flow. The tidal signal is so strong that it reverses the currents near the bottom for a part of each tidal cycle. As a consequence, 2D depth-averaged models have already been applied to simulate surface tides in the Strait (Tejedor et al., 1999). Tsimplis et al. (1995) have even used a 2D barotropic model for simulating tides in the whole Mediterranean Sea.

In the case of the main tidal constituent, M_2, tide amplitude at the Atlantic entrance of the Strait is about 0.8 m. This amplitude decreases towards the east. Thus, at the Mediterranean entrance is only about 0.3 m. The amplitude of the tide is reduced more in the Alborán Sea, reaching 0.09 m at the east limit of our domain (see map in Fig. 2). The associated currents decrease in a similar way: from tidal currents of the order of 1 m/s in the Strait to currents of a few cm/s in the Alborán Sea basin. Similar behaviour is observed for the S_2 constituent.

It has been reported (Auffret et al., 1974) that essentially all the western Alborán basin and southern part of the eastern one (which indeed is the whole domain of the model) are covered with muds, with less than 7% of coarse material (>63 μm). The composition of these muds is controlled by river inputs, marine carbonate production in shallow areas, biogenic production in surface water and water mass circulation (Masqué et al., 2003). Lithogenic particles are mostly introduced to the Alborán Sea by fluvial and eolian mechanisms and, to a small extent, by coastal erosion (less than 5% of the total; see Fabres et al., 2002). Eolian supply is strongly controlled by the proximity of the Sahara Desert. Thus, some episodes of atmospheric dust deposition, mostly of Saharan origin, have been recorded (Fabres et al., 2002). The fluvial input of particles has been extensively investigated by Liquete et al. (2005). These authors have found that supply from the north coast is at least one order of magnitude larger than from the southern one. They provide detailed data on sediment supply by the main rivers discharging into the Alborán Sea.

3. The Alborán Sea model

Currents at any given time and position, which are required to solve the advection terms of the dispersion equation for suspended sediments and radionuclides, are obtained through the addition of the instantaneous tidal current plus the residual flow. Indeed, tides are relevant for the transport of pollutants in the area close to the Strait of Gibraltar, where associated currents are stronger. Inside the Alborán Sea, where weaker tidal currents exist, residual circulation is dominant.

Tidal and residual currents are obtained from two hydrodynamic models working on the same domain: a 2D depth-averaged model is used for calculating tides and a two-layer model is applied to obtain the residual flow. These are reasonable approaches, as discussed above. The hydrodynamic models are run in advance and results are stored in files that will be later used by the dispersion models (suspended sediments and radionuclides).

Nevertheless, the problem is very complicated since, although tides are periodic, the residual flow presents seasonal variability and is also affected by meteorological conditions as pressure differences between the Atlantic and Mediterranean. Winds have to be considered as well. It was decided to run the two-layer model for average inflow and outflow through the Strait of Gibraltar and without wind, thus a constant residual flow is obtained. This may be a too simple approach, but can give a realistic view of the main transport processes in the sea, given the generally good agreement between measured and computed sedimentation rates and radionuclide distributions that will be shown below. However, the sensitivity of suspended sediment and radionuclide transport in the Alborán Sea to changing winds is an interesting problem that has to be addressed in the next future since dispersion processes related to meteorological conditions may become apparent. Moreover, erosion events may be induced by wind waves in the shallower areas. Nevertheless, wave-induced erosion is not included in the model since calculations are carried out under calm conditions. These approaches have been successfully used before when studying the dispersion of suspended particles and radionuclides by the Rhone River plume, northwest Mediterranean Sea (Periáñez, 2005a,b). Following these approaches, the mean particle supplies from the rivers are used (Liquete et al., 2005) and deposition events of Sahara dust are not considered since cannot be quantified. Coastal erosion has finally been neglected in comparison with river supply (Fabres et al., 2002). Only suspended matter is considered in this study, thus bedload transport is not included in the model. Indeed, coarse material transported as bedload has little capacity for adsorbing cations. Finally, only the lithogenic particle fraction is simulated, which accounts about 75−80% of the total suspended load (Fabres et al., 2002; Masqué et al., 2003). The sources of radionuclides will be discussed below.

In spite of all these simplifications, the model retains the essential aspects of water circulation in the Alborán Sea and gives a correct overview of the sedimentation process and radionuclide distributions, as will be shown.

3.1. Hydrodynamic models

A 2D depth-averaged model is used to calculate tidal currents over the domain. Equations are standard and may be seen for instance in Periáñez (2005c). The solution of these equations provides the water currents at each point in the model domain and for each time step. Currents are treated through standard tidal analysis (Pugh, 1987) and tidal constants are stored in files that will be read by the dispersion models to solve the advective terms. The model includes the two main tidal constituents, M_2 and S_2. Thus, the hydrodynamic equations are solved for each constituent and tidal analysis is also carried out for each constituent separately. Some open boundary conditions must be provided to solve the hydrodynamic equations: water surface elevations are specified, from observations, along open boundaries of the computational domain.

Equations are solved using a explicit finite difference scheme (Periáñez, 2005c). The computational domain (Fig. 2) extends from 35°00′ N to 36°56′ N and from 5°54′ W to 2°10′ W. Resolution of the grid is 2 min in longitude and latitude. Water depths were downloaded from the NOAA (US National Ocean and Atmosphere Administration) Geodas database, available on-line. Time step, limited by the CFL (Courant−Friederichs−Lewy) stability condition, is $\Delta t = 10$ s. Once a stable periodic solution is achieved, tidal analysis is carried out to determine tidal constants. This tidal model is the same used in the rapid-response dispersion model for dissolved radionuclides released at the sea surface described in Periáñez (2006).

The residual flow is obtained from a two-layer model. Two water layers with different densities are flowing in opposite directions in the Alborán Sea. Details on the equations describing this flow may be seen, for instance, in Izquierdo et al. (2001).

As commented before, current at a given time and position is obtained through the addition of the instantaneous tidal current plus the residual flow. Tidal currents in the bottom layer are obtained from the depth-averaged tidal current provided by the barotropic model using a standard current profile (Pugh, 1987; Periáñez, 2004a).

The equations of the two-layer model are solved using the same scheme as in the barotropic model. Water flows are specified along open boundaries and equations are integrated until a steady circulation is obtained. Mean surface inflow and deep outflow used to integrate the model are, respectively, 1.25 and 1.20 sverdrup. The inflow magnitude corresponds to the value previously used by Preller (1986) and the outflow is smaller than the inflow by 0.05 sverdrup,

as discussed before. Flows are gradually increased from zero to their maximum values over a finite time to minimize the excitation of high frequency waves (Preller, 1986). Densities of the upper and lower layers are, respectively, 1027 and 1029 kg/m^3 as in Izquierdo et al. (2001).

A summary of the hydrodynamic equations may be seen in Appendix A.

3.2. Sediment transport and radionuclide dispersion

The transport of sediments is described by an advection/diffusion equation for each water layer to which some terms are added. These are external sources of particles, terms describing particle deposition on the seabed and erosion from the bed to the water column, vertical settling and diffusive transport through the interface separating the two water layers. The formulation of these processes is based upon standard formulae. Thus, the erodability constant is used for the erosion term. Particle settling and deposition are described using the settling velocity, which is obtained from Stoke's law. Critical erosion and deposition stresses are used as usually. Details on the mathematical formulation may be seen elsewhere (Periáñez, 2005c; Liu et al., 2002a; Lumborg and Windelin, 2003; Cancino and Neves, 1999) and a summary is given in Appendix A. Finally, it is also possible to calculate net sedimentation rates (SR) as the balance between the deposition and erosion terms.

Non-conservative radionuclides are those which do not remain dissolved in the water column, but have a certain affinity to be fixed to particles. If the radionuclide is introduced in the surface water layer, it will be fixed to settling suspended particles and their deposition on the sea bed will contaminate the bottom sediment. Of course there are also advection/diffusion processes in both water layers, diffusion of dissolved radionuclides and of particles through the pycnocline and direct adsorption of pollutants on the seabed. The exchanges between the dissolved and solid phases may be described in terms of kinetic transfer coefficients. Thus, assuming that adsorption/release reactions are governed by a single reversible reaction, a coefficient k_1 governs the transfer from the liquid to the solid phase and a coefficient k_2 governs the inverse process. Also, the migration of radionuclides to the deep sediment must be included since simulations over several years are carried out. Thus, radionuclides deposited on the sediment surface will be buried by particle deposition and will migrate below the mixed sediment layer that directly interacts with the dissolved phase (see for instance the discussion in Monte et al., 2006). This effect may be easily treated as a decay process with constant λ_{burial} given by:

$$\lambda_{\text{burial}} = \frac{\text{SR}}{\rho_s L} \tag{1}$$

where L is the sediment mixing depth (the distance to which the dissolved phase penetrates the sediment) and ρ_s is the sediment bulk density (dry mass divided by wet volume). A summary of all the processes involved may be seen in Fig. 3.

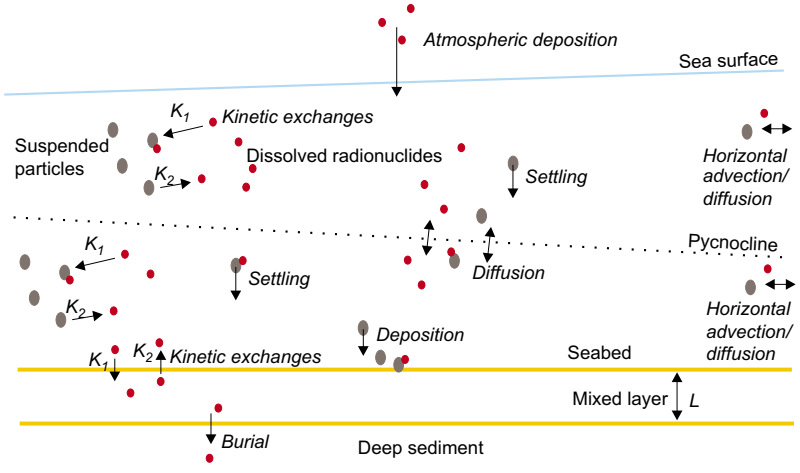

Fig. 3. Processes affecting the dispersion of non-conservative radionuclides in a two-layer sea. Black circles are suspended particles and the red ones are radionuclides. (For interpretation of color in this figure the reader is referred to the web version of the article.)

It is known that adsorption depends on the surface of particles per water volume unit at each point and time. This quantity has been denoted as the exchange surface (Periáñez et al., 1996; Periáñez and Martínez-Aguirre, 1997; Periáñez, 1999, 2000, 2002). Thus, the kinetic coefficient $k_{1,k}$ is written as:

$$k_{1,k} = \chi(S_{\mathrm{m},k} + S_{\mathrm{s}}\delta_{k,2}) = k^{\mathrm{m}}_{1,k} + k^{\mathrm{s}}_{1} \tag{2}$$

where S_{m} and S_{s} are the exchange surfaces for suspended matter and bottom sediments, respectively (dimensions $[\mathrm{L}]^{-1}$) and χ is a parameter with the dimensions of a velocity denoted as the exchange velocity (Periáñez et al., 1996; Periáñez and Martínez-Aguirre, 1997; Periáñez, 1999, 2000, 2002). The index $k = 1, 2$ represents each water layer (surface and bottom, respectively). The delta function is introduced to take into account that only the bottom layer interacts with the bed sediment.

Assuming spherical particles, the exchange surfaces are written as (see references cited above):

$$S_{\mathrm{m},k} = \frac{3m_k}{\rho R} \tag{3}$$

and

$$S_{\mathrm{s}} = \frac{3Lf\phi(1-p)}{RH_2} \tag{4}$$

where R and ρ are particle radius and density, respectively, m_k is the suspended matter concentration in layer k, f is the fraction of small particles in the sediment, p is sediment porosity and ϕ is a correction factor that takes into account that part of the sediment particle surface may be hidden by other sediment particles. Finally, H_2 is the thickness of the bottom water layer. This formulation has been successfully used in all modelling works cited above. Real particles are not spheres, but with this approach it is possible to obtain an analytical expression for the exchange surface (Duursma and Carroll, 1996). The kinetic coefficient k_2 is considered to be constant.

The equation that gives the time evolution of the radionuclide concentration in the dissolved phase, C_{d}, is

$$\begin{aligned}\frac{\partial(HC_{\mathrm{d}})_k}{\partial t} + \frac{\partial(uHC_{\mathrm{d}})_k}{\partial x} + \frac{\partial(vHC_{\mathrm{d}})_k}{\partial y} = {} & \frac{\partial}{\partial x}\left(H_k K_{\mathrm{h}} \frac{\partial C_{\mathrm{d},k}}{\partial x}\right) + \frac{\partial}{\partial y}\left(H_k K_{\mathrm{h}} \frac{\partial C_{\mathrm{d},k}}{\partial y}\right) + \frac{\partial}{\partial z}(K_{\mathrm{v}} C_{\mathrm{d},k}) - k^{\mathrm{m}}_{1,k} H_k C_{\mathrm{d},k} \\ & + k_2 H_k m_k C_{\mathrm{s},k} - k^{\mathrm{s}}_1 H_2 C_{\mathrm{d},2} + \delta_{k,2} k_2 A_{\mathrm{s}} L \rho_{\mathrm{s}} f \phi - \lambda H_k C_{\mathrm{d},k}\end{aligned} \tag{5}$$

where C_{s} and A_{s} are radionuclide concentrations in suspended matter and the bed sediment mixed layer, respectively, and λ is the radioactive decay constant. H is the water layer thickness, u and v water velocity components along the x and y axes, and K_{h} and K_{v} are, respectively, the horizontal and vertical turbulent diffusion coefficients.

The equation for the time evolution of radionuclide concentration in suspended matter is

$$\begin{aligned}\frac{\partial(HC_{\mathrm{s}}m)_k}{\partial t} + \frac{\partial(uHC_{\mathrm{s}}m)_k}{\partial x} + \frac{\partial(vHC_{\mathrm{s}}m)_k}{\partial y} = {} & \frac{\partial}{\partial x}\left(H_k K_{\mathrm{h}} \frac{\partial(C_{\mathrm{s}}m)_k}{\partial x}\right) + \frac{\partial}{\partial y}\left(H_k K_{\mathrm{h}} \frac{\partial(C_{\mathrm{s}}m)_k}{\partial y}\right) + \frac{\partial}{\partial z}(K_{\mathrm{v}} C_{\mathrm{s},k} m_k) \\ & - w_{\mathrm{s},1} m_1 C_{\mathrm{s},1}(\delta_{k,1} - \delta_{k,2}) + k^{\mathrm{m}}_{1,k} C_{\mathrm{d},k} - k_2 m_k C_{\mathrm{s},k} - \delta_{k,2}\mathrm{SR} C_{\mathrm{s},k} \\ & - \lambda H_k m_k C_{\mathrm{s},k}\end{aligned} \tag{6}$$

where w_{s} is particle settling velocity. Finally, for the bed sediment radionuclide concentration we have

$$\frac{\partial A_{\mathrm{s}}}{\partial t} = k^{\mathrm{s}}_1 \frac{H_2 C_{\mathrm{d},2}}{\rho_{\mathrm{s}} L f} - k_2 A_{\mathrm{s}} \phi + \mathrm{SR}\frac{C_{\mathrm{s},2}}{\rho_{\mathrm{s}} L f} - (\lambda + \lambda_{\mathrm{burial}}) A_{\mathrm{s}} \tag{7}$$

in the mixed sediment depth. The total radionuclide content, A_p, in the sediment below the mixed depth is given by the following equation:

$$\frac{\partial A_p}{\partial t} = \lambda_{\mathrm{burial}} \rho_{\mathrm{s}} L f A_{\mathrm{s}} - \lambda A_p \tag{8}$$

The radionuclide concentration in the sediment mixed depth is given by $f A_{\mathrm{s}}$. This is what would be obtained from a surface sediment sample where a coarse sediment fraction $(1 - f)$ exists with negligible radionuclide concentration.

Explicit finite differences are also used to solve the advection/diffusion equation. In particular, the second order accuracy MSOU (Monotonic Second Order Upstream) scheme (Vested et al., 1996) has been applied for the advective terms. A second order scheme is also applied for diffusion (Kowalick and Murty, 1993). The sediment transport model is again integrated until a steady situation is achieved. In practice, simulations over 4 months are carried out. The source of sediment is river supply (from Liquete et al., 2005): the 7 main rivers discharging in the Alborán Sea have been considered. The suspended particle concentration in the inflowing Atlantic waters is fixed as 0.5 g/m^3 (León-Vintró et al., 1999) and a zero gradient condition is used along the other open boundaries. This kind of boundary conditions has already been used in the model described by Tappin et al. (1997).

Values for the diffusion coefficients have to be provided. The horizontal diffusion coefficient depends on the horizontal grid spacing. Following Dick and Schonfeld (1996):

$$K_h = 0.2055 \times 10^{-3} \Delta x^{1.15} \tag{9}$$

The present grid resolution (2 min) gives $K_h = 2.0$ m^2/s. Diffusion through the pycnocline was fixed as $K_v = 1.0 \times 10^{-5}$ m^2/s.

The computed steady distribution of suspended particles and sedimentation rates are again stored in files that are read by the radionuclide dispersion model. Initial and boundary conditions for it are given below.

4. Results

4.1. Hydrodynamics and sediments

A detailed comparison of results of the tidal model with measurements in the Alborán Sea is given in Periáñez (2006) and will not be repeated here.

Parameters required in the two-layer model are summarized in Table 1. The calculated residual flows for the upper and lower layers, for the mean water exchanges through the Strait of Gibraltar, are presented in Fig. 4. In the upper layer, the jet of Atlantic water entering through the Strait of Gibraltar flows towards the east along the Spanish coast and partially curves to the south before reaching Alborán Island. Part of this flow continues to the east between Cape Tres Forcas and Alborán Island and the remaining rotates towards the west. A gyre of anticyclonic circulation is thus

Table 1
Summary of model parameters (two-layer model, sediment and radionuclide dispersion models)

Parameter description	Value	Source
Water density in upper layer	$\rho_1 = 1027$ kg/m^3	Izquierdo et al., 2001
Water density in lower layer	$\rho_2 = 1029$ kg/m^3	Izquierdo et al., 2001
Horizontal eddy viscosity	$A = 50$ m^2/s	Calibration
Interfacial friction	$c_1 = 0.0001$	Calibration
Bed friction	$c_2 = 0.0025$	Calibration
Sediment mixing depth	$L = 0.035$ m	Masqué et al., 2003
Particle density	$\rho = 2600$ kg/m^3	Standard value
Particle radius	$R = 4.0$ μm	Calibration
Fraction of small particles in sediment	$f = 0.95$	Auffret et al., 1974
Correction factor	$\phi = 0.01$	Periáñez and Martínez-Aguirre, 1997
Sediment porosity	$p = 0.6$	Auffret et al., 1974
Horizontal diffusion	$K_h = 2.0$ m^2/s	Dick and Schonfeld, 1996
Diffusion through pycnocline	$K_v = 1.0 \times 10^{-5}$ m^2/s	Standard value
Water kinematic viscosity	$\nu = 1.064 \times 10^{-6}$ m^2/s	Standard value
Erodability	$E = 1.6 \times 10^{-3}$ kg/m^{2}s	Tattersall et al., 2003
Critical erosion stress	$\tau_{ce} = 1.0$ N/m^2	Tattersall et al., 2003
Critical deposition stress	$\tau_{cd} = 0.7$ N/m^2	Tattersall et al., 2003
Desorption kinetic coefficient	$k_2 = 1.16 \times 10^{-5}$ s^{-1}	Nyffeler et al., 1984
Cs distribution coefficient	$k_d = 2$ m^3/kg	Calibration
Pu distribution coefficient	$k_d = 100$ m^3/kg	IAEA, 2004

In the cases of E and the critical stresses for erosion and deposition, the selected values correspond to intermediate values within their range of variation commonly found in literature. A reference (Tattersall et al., 2003) is given as an example.

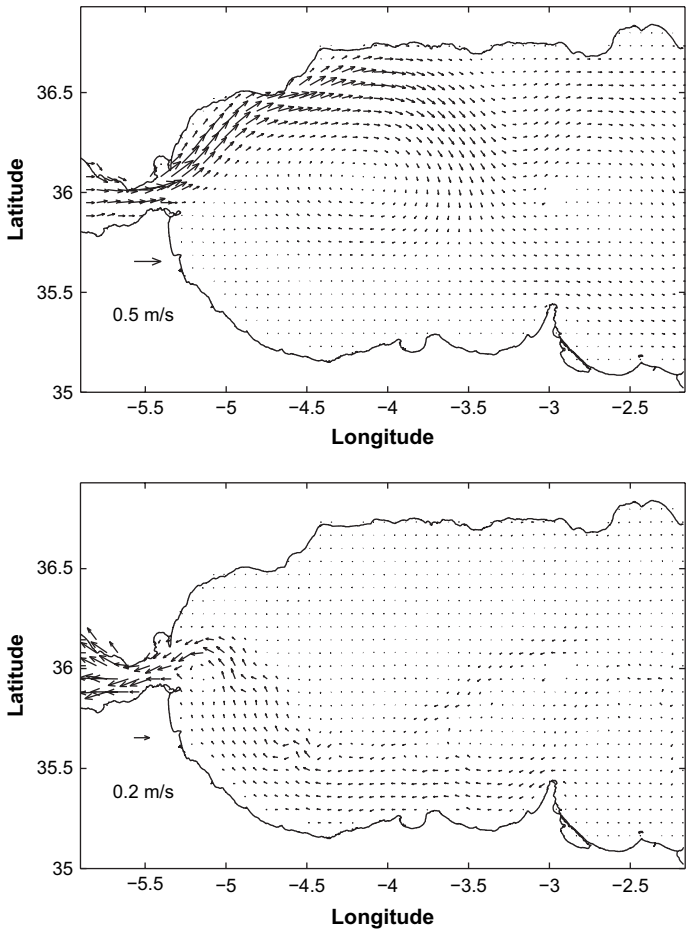

Fig. 4. Computed residual currents in the upper (up) and lower (down) water layers. Only one of each four computed vectors is shown for clarity.

completed. Surface water velocity in the Strait reaches 0.53 m/s, in agreement with the current speeds of the order of 0.6 m/s reported from measurements (Perkins et al., 1990) and models (Sannino et al., 2004). In the jet, along the Spanish coast, maximum surface velocities are of the order of 0.4 m/s. Measurements of Perkins et al. (1990) in this area range between 0.1 and 0.53 m/s and the model of Werner et al. (1988) produces maximum currents in the north of the gyre of 0.25 m/s. Vargas-Yáñez et al. (2002) have measured eastward residual velocities in the passage between Cape tres Forcas and Alborán Island. They are 11 ± 5, 5 ± 3 and 1 ± 3 cm/s at depths of 74, 117 and 178 m, respectively (all depths correspond to the surface layer). Computed current at the same point for the surface layer is 3.8 cm/s.

A westward circulation is obtained for the bottom layer. In the western Strait of Gibraltar computed velocities are of the order of 0.20 m/s, in good agreement with the 0.15 m/s obtained by Béranguer et al. (2005). Maximum outflow current calculated in the Strait is 0.36 m/s; Sannino et al. (2002) obtained a figure of 0.35 m/s. In the Alborán Sea, water velocities are reduced to some 0.1 m/s in the southern area and less in the northern part of the basin. This circulation pattern for the deep layer is in good agreement with the earlier calculations of Preller (1986), that also shows that most of the deep water flows along the south coast with speed below 0.15 m/s, and with measurements in Gascard and Richez (1985), which give velocities in the southern shelf, near the Strait, of 0.1 m/s. As commented before, Bryden and Stommel (1982) have also found that the westward deep flow occurs along the Moroccan continental slope. These authors have measured a mean (using a 341-day record) outflow velocity of 4.6 ± 0.6 cm/s in a point located at about -4.6° longitude and over the 500 m isobath in the Moroccan continental slope. They do not give the exact position of the current meter mooring, but the model predicts (for such longitude and a depth of 535 m) a westward current equal to 3.6 cm/s. In the northern part of the sea, Fabres et al. (2002) have measured

westward currents of 1.93 and 0.95 cm/s in stations C and E (see Fig. 2) respectively. The corresponding calculated currents are 1.0 and 0.60 cm/s.

As expected for geostrophic flow, the interface between both water layers in the Strait of Gibraltar is deeper in the south than in the north. The computed slope along a south−north section at the Atlantic entrance of the Strait is 1.78×10^{-3}, in good agreement with Sannino et al. (2002) who found a value of 1.7×10^{-3}. The thickness of the surface layer is of the order of 200 m.

A summary of parameter values for the sediment transport model is given in Table 1. In particular, since less than 7% of the bed sediments consists of coarse material (Auffret et al., 1974), it has been taken an uniform value of $f = 0.95$. Suspended particles (diameter < 63 μm) are characterized by a mean size that is considered to be representative of suspended matter in this environment. The particle size controls, through Stoke's law, the settling velocity of particles and, as a consequence, affects the sedimentation rate as well. It also affects the adsorption of radionuclides from the dissolved phase (Eqs. (3) and (4)). A sensitivity analysis (not shown) has been carried out, and the selected particle size is that for which the best agreement between measured and calculated sedimentation rates is obtained. The particle diameter finally selected was 8.0 μm. This is a reasonable figure, given that sediments over all the Alborán Sea may be classified as silts (Masqué et al., 2003; Auffret et al., 1974) and consequently particles have diameter in the range 4−63 μm. Moreover, Freitas and Abrantes (2002) have found that particles with diameter <10 μm are dominant in all water masses in the Gulf of Cadiz (the Gulf of Cadiz reflects the Alborán Sea since surface waters in the first flow into the second and Mediterranean waters flow, in the deep layer, from the Alborán Sea into the Gulf of Cadiz). Finally, the selected value is also consistent with Liu et al. (2002b), who used a radius of 2.5 μm to describe fine silts in their model. Of course, it would be convenient to have a detailed particle size spectra and then using several particle classes (Periáñez, 2005b), but it is not available in current literature.

As an example, the map of computed sedimentation rates is shown in Fig. 5. Except in the river plumes, they are of the order of 10^{-2} g/cm^2 year. The smallest SR is obtained in some areas of the Strait of Gibraltar and the Alborán Sea, where larger currents are present in the lower layer and/or stronger tidal currents exist. It is evident from Fig. 5 that a clear structure is produced in SR, which varies over one order of magnitude from the south to the north of the sea. The order of magnitude of the SR is correctly given by the model, although there is a general underestimation of SR over the Alborán Sea. Indeed, measurements are in the range 0.053−0.182 g/cm^2 year (Masqué et al., 2003). This is not surprising given the approximations made in the model: episodes of heavy rains, atmospheric deposition and bedload are not included. Moreover, only the lithogenic particle fraction, which is about 80% of the total suspended load as commented above, is simulated.

Masqué et al. (2003) have concluded, from their set of measurements, that there is a general trend by which SR decreases as the water column depth increases, specially in the area of Málaga. Model results show this effect; indeed

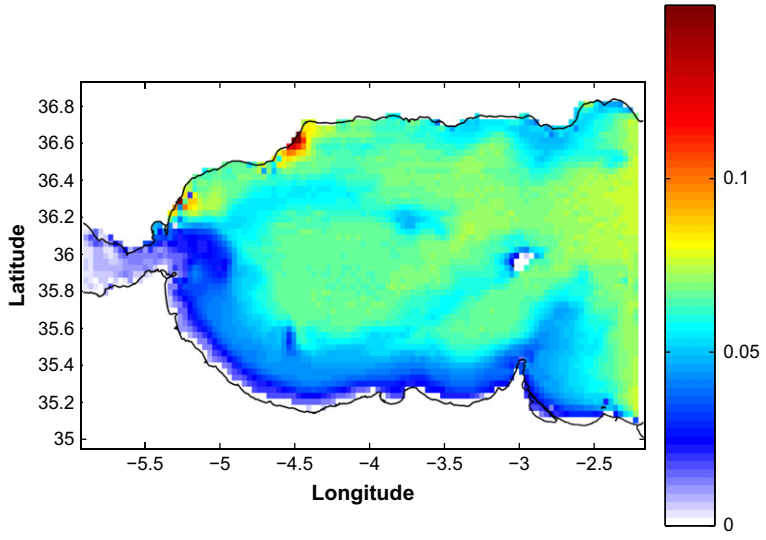

Fig. 5. Computed sedimentation rates (g/cm^2 year) over the model domain.

it may be seen in Fig. 5 that higher SR in the Málaga area appears to be due to the influence of river discharges and the Atlantic jet. Nevertheless, the opposite effect is present along the south coast of the Alborán Sea: here SR increases with distance from the coast. Although there are not measurements in this area, model results are consistent with the fact that higher currents (and hence lower SR) exist close to the southern coast in the lower water layer. Moreover, this area is far from the main sediment sources in the model (Spanish rivers and Gibraltar inflow) and, consequently, most particles will be deposited before reaching the south of the Alborán Sea.

Particle concentrations in the upper layer are about 0.4 g/m^3 in the Strait of Gibraltar and in the Atlantic jet in the Alborán Sea. Concentration decreases in the WAG and in the south part of the sea to some 0.2 g/m^3. Slightly higher concentrations, about 0.4−0.5 g/m^3, are obtained in most of the bottom layer. These values are in agreement with León-Vintró et al. (1999), who found suspended particle concentrations below 0.5 g/m^3 in several stations sampled in the Strait of Gibraltar and Alborán Sea (exact values of concentrations are not reported in such paper). Also, Freitas and Abrantes (2002) have measured suspended matter concentrations in Mediterranean waters, in the Atlantic entrance of the Strait and in the Gulf of Cadiz, which are always smaller than 0.94 g/m^3.

4.2. Radionuclide distribution

As commented before, the model has been applied to ^{137}Cs and ^{239,240}Pu. Values for parameters describing radionuclide transport are summarized in Table 1. Those which describe the geochemical behaviour of the different radionuclides are the exchange velocity χ and the kinetic transfer coefficient for the desorption process k_2.

The correction factor ϕ has been fixed as 0.01 according to previous modelling works (Periáñez and Martínez-Aguirre, 1997). Sediment porosity is 0.6 according to the measurements in Auffret et al. (1974).

In the case of ^{137}Cs, the kinetic coefficient k_2 is 1.16×10^{-5} s^{-1} according to the experiments in Nyffeler et al. (1984), value that has been used in other modelling works concerning this radionuclide (Periáñez, 2000, 2005b,c). The exchange velocity has been obtained from the equation relating this parameter with k_2 and the equilibrium distribution coefficient, k_d (Periáñez and Martínez-Aguirre, 1997; Periáñez, 2005a−c):

$$k_d = \frac{\chi}{k_2}\frac{3}{\rho R} \tag{10}$$

The k_d mean value recommended by the International Atomic Energy Agency is 4 m^3/kg (IAEA, 2004) for Cs, although it may vary in more than one order of magnitude depending on environmental conditions. In the present application, the value that has been used is $k_d = 2$ m^3/kg since a better agreement with observations is obtained. Nevertheless, the model sensitivity to this parameter is studied in Section 4.4. Since R, k_d and k_2 are already defined, the value of χ is determined from Eq. (10).

As described in Nyffeler et al. (1984), k_2 is very similar even for radionuclides with a rather different geochemical behaviour, being k_1 the essential parameter describing the tracer geochemical behaviour. Thus the value given to k_2 for ^{239,240}Pu is the same as used for ^{137}Cs. Then the χ value (and hence k_1 from Eqs. (3) and (4)) for this radionuclide is obtained from Eq. (10) using its corresponding recommended k_d, which is 100 m^3/kg (IAEA, 2004). This procedure has been successfully used before (Periáñez and Martínez-Aguirre, 1997; Periáñez, 1999, 2000, 2005a).

Nevertheless, it has to be considered that the behaviour of Pu in aquatic systems is of considerable complexity due to the fact that can exist in different oxidation states simultaneously. The reduced Pu [Pu(III) and Pu(IV)] is highly particle-reactive and has been shown to possess a k_d that is approximately two orders of magnitude higher than that of the more soluble oxidized Pu [Pu(V) and Pu(VI)]. Different exchange velocities should be used for oxidized and reduced Pu, as has been done in Periáñez (2003). However, in this work different plutonium oxidation states have not been considered due to the lack of experimental data on Pu speciation in the area. Thus, measurements represent the mixture of oxidation states that is present in the particular sample. A measured effective k_d, representative of such mixture, is used to obtain an effective exchange velocity. This approach for simulating Pu dispersion is used in other models (Periáñez, 1999; Aldridge et al., 2003). Moreover, the vertical transport of plutonium related to the settling of biogenic particles cannot be simulated by the model since only the lithogenic particle fraction is considered, as mentioned before. Thus, the results for plutonium have to be considered only as a first approach to a very complex problem. Nevertheless, these results are of interest to show the very different dynamics of radionuclides depending on their geochemical behaviour (the very different reactivity of Cs and Pu).

In the case of ^{137}Cs, the model has been run for the period 1985 (one year before Chernobyl accident) to 1997, when computed ^{137}Cs concentrations in the bed sediment are compared with measurements in Masqué et al. (2003). Initial ^{137}Cs concentrations for both water layers are obtained from the long-term box model of Sánchez-Cabeza et al. (2002) and are assumed to be homogeneous over the entire domain. They are 3.0 and 2.0 Bq/m^3 for the upper and lower layer, respectively. Concentrations in suspended matter and bottom sediments are assumed to be initially in equilibrium with the dissolved phase. Atmospheric and Chernobyl inputs are obtained from Sánchez-Cabeza et al. (2002) as well.

The computed distribution of ^{137}Cs in the surface bed sediments at the end of the simulation may be seen in Fig. 6 and a comparison with measurements in Masqué et al. (2003) and Gascó et al. (2002b) is presented in Table 2 (column corresponding to $k_d = 2$ m^3/kg). It seems from the table that the model gives uniform ^{137}Cs concentrations in the sediment. This is just an effect of the specific locations of sampling points and, indeed, a clear structure is produced (see Fig. 6). Computed concentrations are in the range 3−6 Bq/kg (the color scale in Fig. 6 is limited to 5 Bq/kg for more clarity), in generally good agreement with measurements (Table 2). (For interpretation of color in this figure the reader is referred to the web version of the article.) There are higher concentrations along both coasts of the Alborán Sea, particularly along the Spanish coast, where SR are higher due to the riverine input of particles. Thus, it could be deduced that ^{137}Cs incorporated to the surface water from the atmosphere is attached to suspended particles that are later deposited on the bed. Indeed, lower concentrations are in general obtained in the Strait of Gibraltar and along the main path followed by the deep outflow current, where SR are smaller. Nevertheless, direct adsorption of ^{137}Cs from the dissolved phase to the bed sediment is occurring simultaneously and an absolutely clear correlation between SR and ^{137}Cs concentration in sediments cannot be established. Indeed, direct adsorption is higher in shallower areas, as can be seen from Eq. (4), and consequently the map in Fig. 6 is affected by topography with a general trend of increasing ^{137}Cs concentrations with decreasing water depth. Moreover, direct adsorption of radionuclides (and trace metals in general) is affected by the water−sediment contact time (Benes et al., 1992). Thus, direct adsorption is smaller in regions of stronger currents in the bottom water layer, as is the case with SR. It may be concluded that a clear correlation between contamination of the bed sediment and SR cannot be established, although a correct estimation of SR is of course required for an appropriate simulation of particle-reactive radionuclide transport.

The mean inventory of ^{137}Cs in bed sediments over the Alborán Sea has been calculated as well. This inventory includes radionuclides in the surface sediments plus radionuclides that have migrated down the sediment core according to Eqs. (1) and (8). The obtained value, 158 Bq/m^2 (Table 2) is in good agreement with the estimations carried out by Gascó et al. (2002b) from measurements: these authors have obtained an inventory of 163 ± 10 Bq/m^2 in the area of Málaga. The computed total inventory in bed sediments is 6.70 TBq. The total inventory in the water column (for both layers) has been calculated as well, resulting 75.2 TBq. However, there are not experimental estimations to compare with in this case.

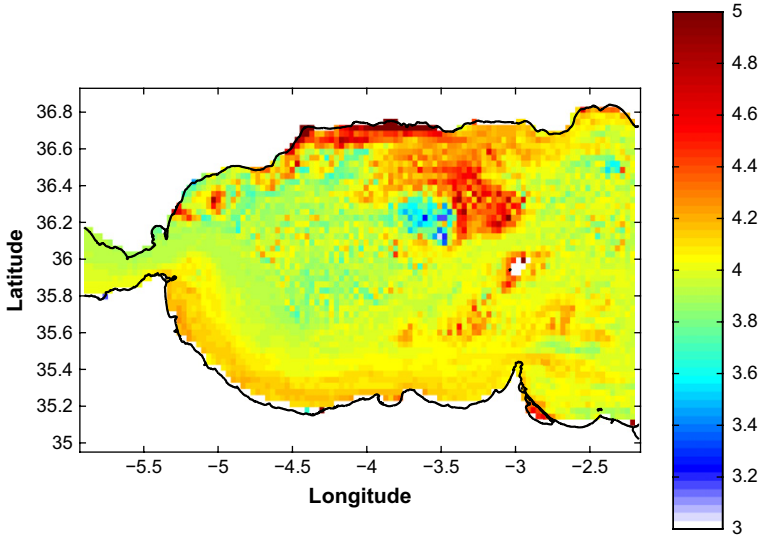

Fig. 6. Computed distribution of ^{137}Cs (Bq/kg) in surface bed sediments of the Alborán Sea.

Table 2
Measured and computed ^{137}Cs concentrations (Bq/kg) in surface sediments of the Alborán Sea at some positions and for several k_d values

Station	Measured	$k_d = 1$ m^3/kg	$k_d = 2$ m^3/kg	$k_d = 4$ m^3/kg
A	2.6 ± 1.2	1.92	3.85	7.75
C	2.5 ± 1.5	1.95	3.92	7.88
E	7.3 ± 2.2	1.93	3.91	7.83
G	3.2 ± 1.9	1.95	3.89	7.79
H	5 ± 3	2.00	3.99	7.99
J	2.8 ± 0.5	1.95	3.93	7.97
Inventory	163 ± 10	79	158	318

The mean sediment inventory is given in Bq/m^2. The nominal simulation corresponds to $k_d = 2$ m^3/kg, the other results are discussed in Section 4.4.

Gascó et al. (2002a) have measured ^{137}Cs concentrations in unfiltered water samples from the Strait of Gibraltar (surface and deep water) in 1997. Model results have also been compared with these measurements. Results are presented in Table 3, where it may be seen that the model gives realistic results for the water column as well. Essentially the same ^{137}Cs concentrations are computed in surface and deep waters, in agreement with measurements of Gascó et al. (2002a).

In the case of ^{239,240}Pu, a simulation over 20 years has been carried out. The atmospheric deposition has been compiled from León-Vintró et al. (1999) and Hirose et al. (2003), and zero activity concentrations in all phases are considered as initial conditions for the simulation. The computed distribution of Pu in the sediment may be seen in Fig. 7. It can be clearly seen that this distribution is rather different to that of Cs, which is due to the different geochemical behaviour of both radionuclides. Only one measurement has been found to compare model results. Measured ^{239,240}Pu concentration in the surface sediment at point J (León-Vintró et al., 1999) is 0.550 Bq/kg, and the computed one is 0.379 Bq/kg.

The computed radionuclide concentrations corresponding to unfiltered water are presented for both water layers in Figs. 8 and 9, for ^{137}Cs and ^{239,240}Pu, respectively. The distributions in the upper layer are similar for both radionuclides, showing higher concentrations in the area occupied by the WAG. This is due to the fact that some water is trapped in the gyre and thus its radionuclide concentration increases as a result of the atmospheric input. Nevertheless, simulations are made under steady flow conditions, thus this pattern will be destroyed by episodes of migration and disappearance of the WAG and winds. However, it is worth commenting that the pattern of higher radionuclide concentrations (for ^{210}Pb, introduced by atmospheric deposition as well) in the centre of the oceanic gyres (in both the Pacific and North Atlantic) has already been detected (Ivanovich and Harmon, 1992, page 384). Consequently, the radionuclide enhancement in the WAG is a real process, although overestimated because of the simulation conditions (steady residual flow).

Table 3
Computed and measured total concentrations in the water column (dissolved plus suspended matter) of ^{137}Cs (Bq/m^3) and ^{239,240}Pu (mBq/m^3) at several locations

Station		Measured		Computed	
		^{137}Cs	^{239,240}Pu	^{137}Cs	^{239,240}Pu
J	Surface		10.0 ± 0.4		6.97
	Deep		23 ± 5		12.9
L	Surface	3.1 ± 0.3	14.1 ± 1.5	3.02	6.9
	Deep	2.1 ± 0.3	18.0 ± 1.6	1.99	13.0
M	Surface	2.62 ± 0.24	9.5 ± 1.2	3.02	6.9
	Deep	2.2 ± 0.3	23.1 ± 1.7	1.98	13.7
N	Surface		11.1 ± 0.4		7.7
	Deep		21.5 ± 2.1		13.2
P	Surface		12 ± 5		45.7
	Deep		19.2 ± 2.1		14.9
Q	Surface		4.8 ± 0.3		6.8
	Deep		20.9 ± 0.7		12.6

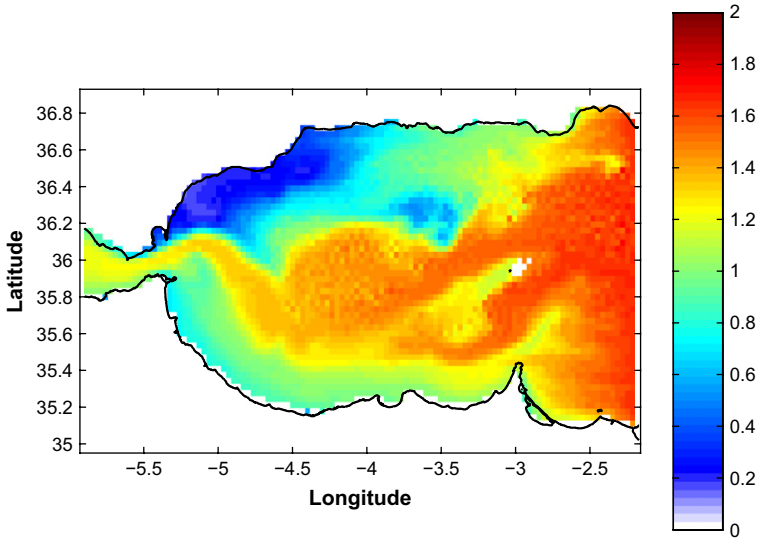

Fig. 7. Computed distribution of ^{239,240}Pu (Bq/kg) in surface bed sediments of the Alborán Sea.

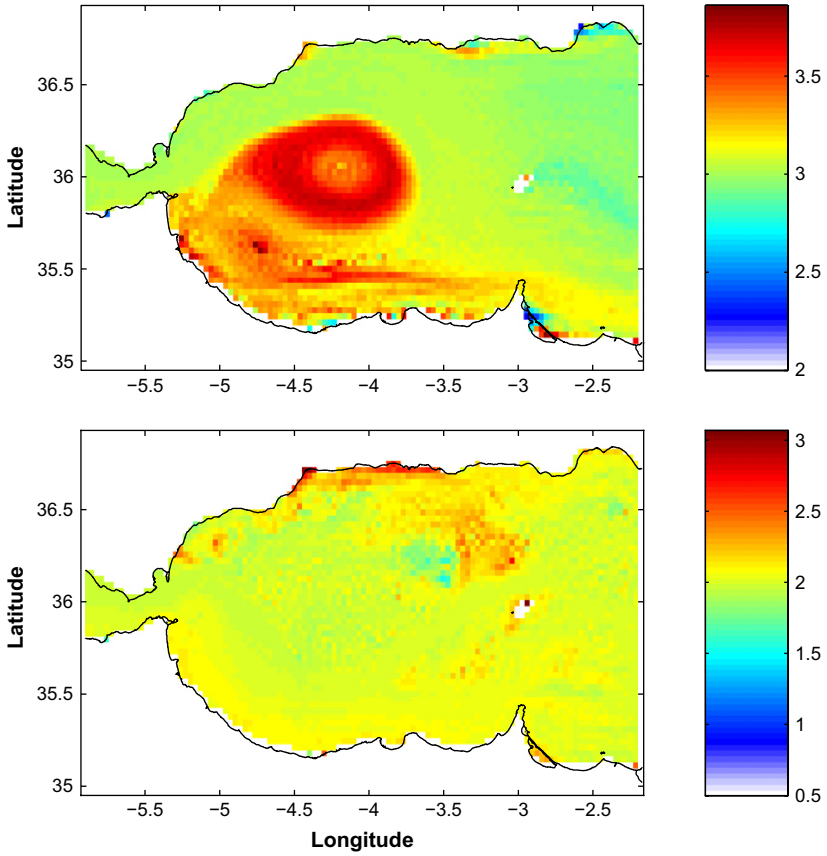

Fig. 8. Computed ^{137}Cs concentrations in unfiltered water (Bq/m^3) in the upper and lower water layers (up and down, respectively).

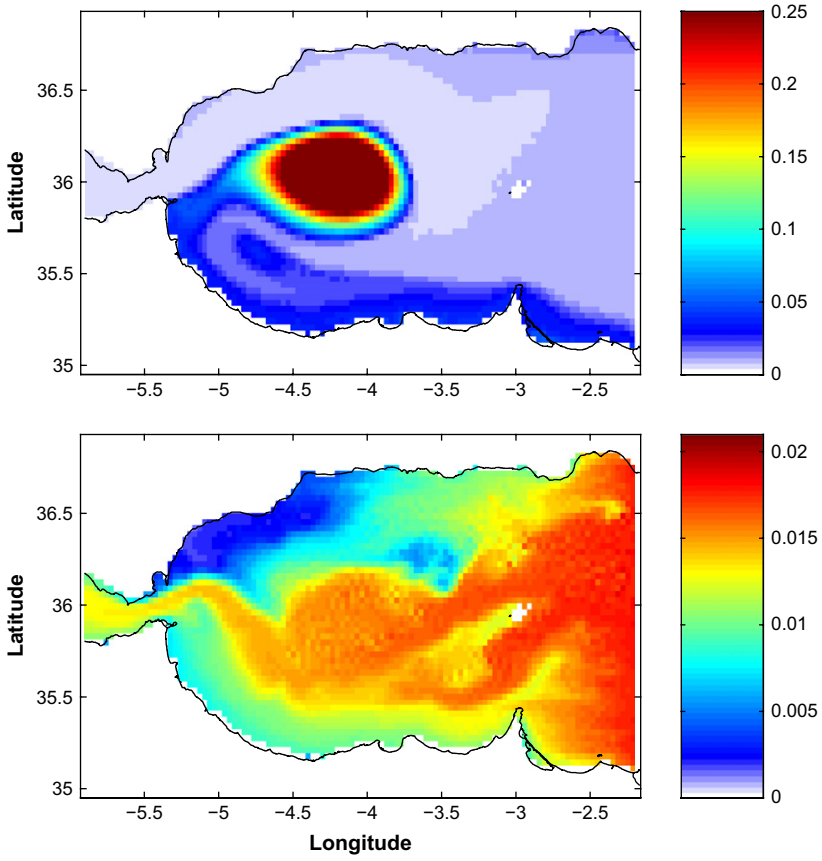

Fig. 9. Computed ^{239,240}Pu concentrations in unfiltered water(Bq/m^3) in the upper and lower water layers (up and down, respectively).

In the case of a highly reactive radionuclide as ^{239,240}Pu, it is quickly fixed to suspended matter and then, by settling, introduced into the deep water layer. Finally radionuclides are deposited on the seabed. Although it cannot be clearly seen in Fig. 9 because of the scale in the colorbar, it is evident from Table 3 that computed concentrations in the deep layer are about a factor 2 higher than in the surface layer. (For interpretation of color in this figure the reader is referred to the web version of the article.) This result is in agreement with the observations presented in Table 3, although the model is slightly underestimating concentrations.

Thus, in the lower layer, distributions are clearly different for both radionuclides due to the different efficiency of the removal process of dissolved radionuclides by settling suspended particles. In fact we can clearly see now that radionuclide distributions in sediments are correlated with those in the deep (unfiltered) water. This is not surprising since deposition of radionuclides on the sediment depend on the radionuclide concentration in suspended matter, and the direct adsorption of radionuclides by the sediment depends on the radionuclide concentration in dissolved form in the deep layer.

The computed average inventory of ^{239,240}Pu over the model domain in the sediment is 45.8 Bq/m^2. Gascó et al. (2002b) have obtained a value of 29 ± 2 Bq/m^2, although only one sediment core was analyzed. Consequently, it can just be said that the order of magnitude seems correct. The total inventory in the sediment results 1.9 TBq. The computed inventory of ^{239,240}Pu in the water column is 0.68 TBq, which agrees with the estimation of 0.64 TBq in León-Vintró et al. (1999). However, this agreement should be interpreted with care since we have seen that the model tends to underestimate Pu concentrations in the water column. Thus, there must be a concentration overestimation somewhere in the sea. This area must be the WAG, because of the steady flow conditions used in the simulation as commented above. This seems confirmed by the surface sample at point P (see Table 3).

The computed fractions of ^{239,240}Pu in the dissolved phase may be seen in Fig. 10 for both water layers. Most of it remains dissolved in spite of the strong affinity of plutonium to be fixed to the solid phase, which is due to the low

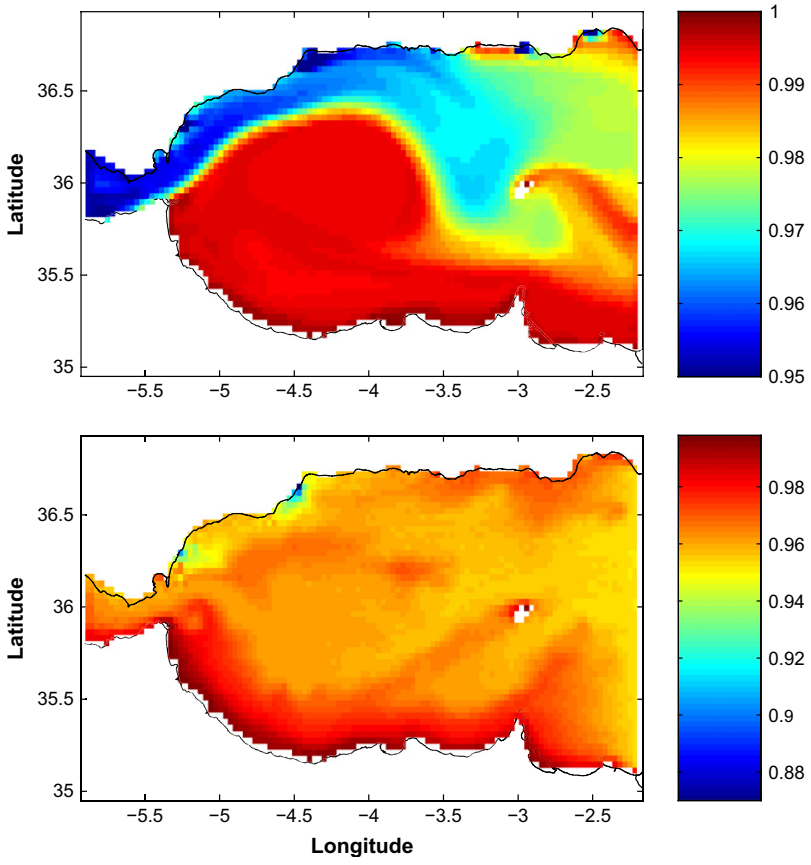

Fig. 10. Computed fraction of dissolved ^{239,240}Pu in the upper and lower water layers (up and down, respectively).

suspended particle concentrations in the Alborán Sea. Thus, in the surface layer the fraction of plutonium in particles ranges from values of the order of 1% in the WAG to some 4−5% in the Atlantic jet. In the deep layer this fraction is about 4% for most of the sea, except in the plumes of the main rivers where suspended particle concentrations are higher. These results are in good agreement with León-Vintró et al. (1999), who found that the percentage of ^{239,240}Pu in particulate form is in the range 2−4%.

The model uses the distribution coefficient for calculating the exchange velocity for each radionuclide, as described above (Eq. (10)). However, the partition of radionuclides between the liquid and solid phases has not to be in equilibrium necessarily. Indeed, the model can calculate the k_d that would be measured from a sample as the ratio between radionuclide concentrations in the solid and dissolved phases. As an example, the computed water-suspended matter k_ds for ^{137}Cs and ^{239,240}Pu in the upper water layer are presented in Fig. 11. In most of the sea radionuclide partition is at equilibrium since the computed k_d is essentially the same value used in Eq. (10) to obtain the exchange velocity (100 and 2 m^3/kg for Pu and Cs, respectively, as discussed before). However, the system is slightly out from equilibrium in the area of the Strait of Gibraltar. This is probably due to the strong currents that are present here in the upper layer, which do not allow radionuclide partition to reach equilibrium. This effect is not observed in the lower water layer, where radionuclide partition is at equilibrium over all the Alborán Sea and the Strait. Currents are weaker in this layer.

4.3. Radionuclide fluxes through the Strait of Gibraltar

The fluxes of the two studied radionuclides through the Strait of Gibraltar (through a north−south section at the longitude of Tarifa) have been evaluated from the model results. Indeed, several estimations of fluxes for some

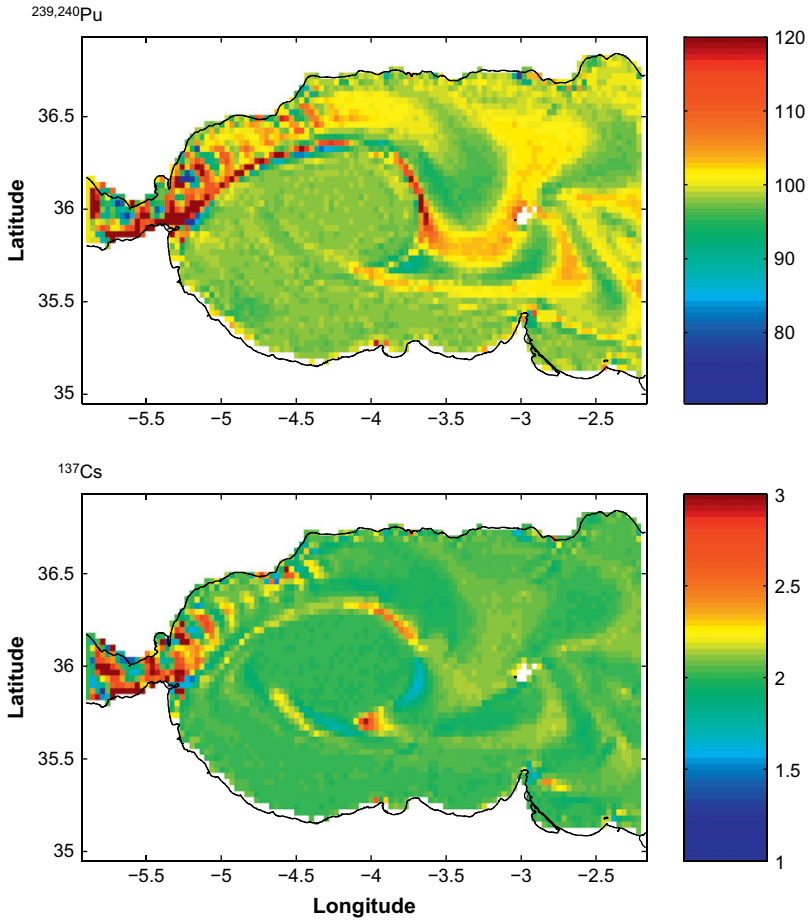

Fig. 11. Computed ^{239,240}Pu and ^{137}Cs water-suspended matter distribution coefficient (m^3/kg) in the upper water layer.

radionuclides and metals have already been done from measurements (Van Geen and Boyle, 1990; Elbaz-Poulichet et al., 2001; León-Vintró et al., 1999; Gascó et al., 2002a; Gómez, 2003).

The water transport used in the estimations ranged from 0.69/0.65 sverdrup (inflow/outflow) (used by Sarmiento et al., 1988) to 1.77/1.73 sverdrup (used by Greze et al., 1985). As a consequence of the variability of the water exchanges in the literature, radionuclide and metal fluxes may present differences up to a factor 3 for the same concentration of the substance (Gómez, 2003). A comparison of the model calculations with previous estimations may be seen in Table 4, where the water exchanges used in each calculation are also given. In spite of the variability of the water exchanges all results are in reasonable agreement and differences reach a factor 2 as maximum. In general, it seems that the model calculation tends to overestimate the inflow of ^{137}Cs. It should be taken into account, however, that estimations are sometimes based on a single measurement of radionuclide concentration in the Strait.

Table 4
Annual fluxes of radionuclides (TBq) in the Atlantic (F_{in}) and Mediterranean (F_{out}) waters through the Strait of Gibraltar

^{137}Cs		^{239,240}Pu		Inflow/outflow	Source
F_{in}	F_{out}	F_{in}	F_{out}		
118	75	0.27	0.44	1.25/1.20	1
72 ± 18	60 ± 13	0.28 ± 0.11	0.62 ± 0.16	0.90/0.90	2
		0.22	0.87	1.39/1.32	3
64	51	0.25	0.53	0.81/0.76	4

Water exchanges (inflow/outflow) are given in sverdrup. Sources of data are the following: 1, the present model; 2, Gascó et al. (2002a); 3, León-Vintró et al. (1999); 4, Gómez (2003).

4.4. Sensitivity analysis

Some sensitivity analysis have been carried out to study the model response to changes in parameters which are poorly defined. In particular, the case of the distribution coefficient is discussed here. The sensitivity analysis have been made for the case of ^{137}Cs since simulation times are shorter and because a k_d value different to the IAEA recommended one has been used.

Obviously, a higher k_d means that the substance has a higher affinity to be fixed to the solid phase and vice versa. Both the surface sediment concentrations and total inventories are linearly correlated with the k_d, as should be expected from the model formulation. It may be seen in Table 2 that computed ^{137}Cs concentrations in the surface sediment are well above the measured levels if the average k_d value given by the IAEA, 4 m^3/kg (IAEA, 2004), is used. Computed concentrations diminish as the k_d is reduced and, in general, the best agreement with measurements is obtained with a k_d equal to 2 m^3/kg. Indeed, the sediment inventory is clearly underestimated if a k_d of 1 m^3/kg is used, although ^{137}Cs concentrations in the surface sediment are acceptable. A detailed study, by means of Monte Carlo methods, of the sensitivity of the description of the water−sediment interactions to the different parameters involved may be seen in Periáñez (2004b) and will not be repeated here.

5. Conclusions

The dynamics of ^{137}Cs and ^{239,240}Pu in the Alborán Sea has been studied by means of numerical modelling. The model consists of three sub-models describing hydrodynamics, sediment transport and radionuclide dispersion. The Alborán Sea has been treated as a two-layered system, and an appropriate description of radionuclide transport in it has been developed. The hydrodynamic models (2D depth-averaged and two-layer for tides and mean flow, respectively) and the sediment transport model for a two-layered sea have been described before. Uptake/release radionuclide reactions between the liquid and solid phases are described by means of kinetic transfer coefficients.

Computed and measured radionuclide concentrations in the water column and in bed sediments have been compared. Different behaviours are observed for Cs and Pu due to their different geochemistry. Generally speaking, the model produces results in agreement with measurements. A correct estimation of ^{137}Cs levels in bed sediments and in the water column is made. Also, the model reproduces the observed fact that essentially the same Cs concentrations exist in both water layers. Although the model slightly underestimates Pu concentrations in the water column, it is obtained that concentrations in the deep water layer are essentially a factor 2 higher than in the surface layer because of the efficient removal of dissolved plutonium by settling suspended particles. The partition of plutonium between water and suspended matter is correctly given by the model: less than 5% of plutonium is fixed to suspended particles. This small value is due to the low suspended matter concentrations existing in this environment. Radionuclide partition is found to be at equilibrium over all the sea except in the upper water layer in the Strait of Gibraltar. This is probably due to the strong currents in this area.

An interesting effect has been observed. It consists of an enhancement of radionuclide concentrations in the WAG. This effect has also been observed in the centre of oceanic gyres in the Atlantic and Pacific. It is due to the fact that water remains trapped in the gyre region, remaining relatively isolated from the surroundings, and thus accumulating radionuclides introduced from the atmosphere. This pattern may be broken by fluctuations of the mean flow, as episodes of disappearance of the WAG, and by winds. Consequently, the accumulation effect, although real, is overestimated by the model.

Radionuclide fluxes through the Strait of Gibraltar have been finally evaluated. They are in relative good agreement with previous estimations based upon radionuclide concentration measurements in the Strait.

Acknowledgements

Work supported by the Research Project of Excellence RNM-419 *Técnicas Ultrasensibles para la Determinación de Radionucleidos en Muestras Ambientales*, Junta de Andalucía, Spain. The author is indebted to the Spanish Ministerio de Educación y Ciencia for a fellowship to stay during three months at the University of Wales, Bangor, where part of this work was carried out, and to Dr. Pere Masqué, from the Universidad Autónoma de Barcelona, for kindly providing some data on ^{137}Cs in bed sediments.

Appendix A. Hydrodynamic and sediment transport equations

The 2D depth-averaged equations used to calculate tides over the domain are

$$\frac{\partial(H\overrightarrow{u})}{\partial t}+\nabla(H\overrightarrow{u}\cdot\overrightarrow{u})+\Omega\overrightarrow{k}\times H\overrightarrow{u}+gH\nabla\zeta=-\overrightarrow{\tau}/\rho_{\mathrm{w}}+AH\nabla^2\overrightarrow{u} \tag{11}$$

$$\frac{\partial H}{\partial t}+\nabla\cdot H\overrightarrow{u}=0 \tag{12}$$

where $\overrightarrow{u}$ is the tidal velocity vector with components (u, v) along the x and y axes, H is total water depth, $H=D_0+\zeta$, where D_0 is the mean water depth and ζ is the displacement of the water surface with respect to the mean level, and Ω is the Coriolis parameter. ρ_{w} is the average water density, A is a horizontal friction coefficient and ∇ is the horizontal gradient operator.

The friction stress $\overrightarrow{\tau}$ is solved in components τ_u and τ_v, which have been written in terms of a quadratic law:

$$\tau_u=k\rho_{\mathrm{w}}u\sqrt{u^2+v^2}$$

$$\tau_v=k\rho_{\mathrm{w}}v\sqrt{u^2+v^2} \tag{13}$$

where k is the bed friction coefficient.

The two-layer model equations describing residual mean flow are

$$\frac{\partial(H_1\overrightarrow{u}_1)}{\partial t}+\nabla(H_1\overrightarrow{u}_1\cdot\overrightarrow{u}_1)+\Omega\overrightarrow{k}\times H_1\overrightarrow{u}_1+gH_1\nabla\zeta_1=-\overrightarrow{\tau}_1/\rho_1+AH_1\nabla^2\overrightarrow{u}_1 \tag{14}$$

$$\frac{\partial H_1}{\partial t}+\nabla\cdot H_1\overrightarrow{u}_1=0 \tag{15}$$

$$\frac{\partial(H_2\overrightarrow{u}_2)}{\partial t}+\nabla(H_2\overrightarrow{u}_2\cdot\overrightarrow{u}_2)+\Omega\overrightarrow{k}\times H_2\overrightarrow{u}_2+g\frac{\rho_1}{\rho_2}H_2\nabla\zeta_1+g'H_2\nabla\zeta_2=(\overrightarrow{\tau}_1-\overrightarrow{\tau}_2)/\rho_2+AH_2\nabla^2\overrightarrow{u}_2 \tag{16}$$

$$\frac{\partial H_2}{\partial t}+\nabla\cdot H_2\overrightarrow{u}_2=0 \tag{17}$$

with indexes 1 and 2 for the upper and lower layers, respectively. In these equations H_k is the thickness of the water layer, ρ_k is water density in each layer, A is a horizontal friction coefficient and g' is the reduced-gravity:

$$g'=g\frac{\rho_2-\rho_1}{\rho_2} \tag{18}$$

ζ_1 is the elevation of the sea surface with respect to the mean level and ζ_2 is the depth of the interface between layers. Finally $\overrightarrow{\tau}_1$ and $\overrightarrow{\tau}_2$ are friction stresses between water layers and between the lower layer and the seabed, respectively. They are again formulated in term of a quadratic law:

$$\overrightarrow{\tau}_1=c_1\rho_1|\overrightarrow{u}_1-\overrightarrow{u}_2|(\overrightarrow{u}_1-\overrightarrow{u}_2)$$

$$\overrightarrow{\tau}_2=c_2\rho_2|\overrightarrow{u}_2|\overrightarrow{u}_2 \tag{19}$$

where c_1 and c_2 are the interfacial and bottom friction coefficients.

The equation for suspended sediment transport is

$$\frac{\partial(Hm)_k}{\partial t}+\frac{\partial(uHm)_k}{\partial x}+\frac{\partial(vHm)_k}{\partial y}=\frac{\partial}{\partial x}\left(H_kK_{\mathrm{h}}\frac{\partial m_k}{\partial x}\right)+\frac{\partial}{\partial y}\left(H_kK_{\mathrm{h}}\frac{\partial m_k}{\partial y}\right)-w_{\mathrm{s},1}m_1(\delta_{k,1}-\delta_{k,2})+\frac{\partial}{\partial z}(K_{\mathrm{v}}m_k)$$
$$+(\mathrm{ER}-\mathrm{DEP})\delta_{k,2}+S\delta_{k,1} \tag{20}$$

where $k = 1, 2$ for the upper and lower layers, respectively, m_k is the suspended matter concentration, u_k and v_k are layer-averaged currents, K_h and K_v are the diffusion coefficients, respectively, for horizontal mixing and mixing through the pycnocline, S is the external particle source and ER and DEP are the erosion and deposition terms, respectively. The settling velocity of particles $w_{s,k}$ is different for each layer due to the different water density and delta functions are introduced to consider that erosion and deposition processes only affect to the bottom water layer and that the external sources, due to river supplies, are introduced into the upper layer.

The deposition term is written in the following form:

$$\mathrm{DEP} = w_{s,2} m_2 \left(1 - \frac{|\overrightarrow{\tau}|}{\tau_{cd}}\right) \tag{21}$$

where $\overrightarrow{\tau}$ is the total bottom friction stress (tides plus mean flow) and τ_{cd} is a critical deposition stress above which no deposition occurs since particles are kept in suspension by turbulence. The settling velocity of particles is obtained from Stokes's law:

$$w_{s,k} = \frac{\rho - \rho_k}{\rho_k} \frac{gD^2}{18\nu} \tag{22}$$

where ρ and D are suspended particle density and diameter, respectively, and ν is the kinematic viscosity of water.

The erosion rate is written in term of the erodability constant:

$$\mathrm{ER} = Ef \left(\frac{|\overrightarrow{\tau}|}{\tau_{ce}} - 1\right) \tag{23}$$

where E is the erodability constant, f gives the fraction of small particles (diameter less than 62.5 μm) in the bed sediment (which are particles that may be resuspended) and τ_{ce} is a critical erosion stress below which no erosion occurs.

References

Aldridge, J.N., Kershaw, P., Brown, J., McCubbin, D., Leonard, K.S., Young, E.F., 2003. Transport of plutonium (^{239}/^{240}Pu) and caesium (^{137}Cs) in the Irish Sea: comparison between observations and results from sediment and contaminant transport modelling. Continental Shelf Research 23, 869−899.

Auffret, G.A., Pastouret, L., Chamley, H., Lanoix, F., 1974. Influence of the prevailing current regime on sedimentation in the Alborán Sea. Deep Sea Research 21, 839−849.

Benes, P., Cernik, M., Lam-Ramos, P., 1992. Factors affecting the interaction of radiocesium with freshwater solids. Contact time, concentrations of solids and temperature. Journal of Radioanalytical and Nuclear Chemistry 159, 201−218.

Béranguer, K., Mortier, L., Crépon, M., 2005. Seasonal variability of water transport through the Straits of Gibraltar, Sicily and Corsica, derived from a high-resolution model of the Mediterranean circulation. Progress in Oceanography 66, 341−364.

Bryden, H.L., Stommel, H.M., 1982. Origin of the Mediterranean outflow. Journal of Marine Research 40, 55−71.

Bryden, H.L., Candela, J., Kinder, T.H., 1994. Exchange through the Strait of Gibraltar. Progress in Oceanography 33, 201−248.

Cancino, L., Neves, R., 1999. Hydrodynamic and sediment suspension modelling in estuarine systems. Part I: Description of the numerical models. Journal of Marine Systems 22, 105−116.

Castro-Díaz, M.J., Macías-Sánchez, J., Parés, C., 1994. Un modelo multicapas de aguas poco profundas. Aplicación al mar de Alborán. In: Parés, C., Valle, A. (Eds.), Modelado de Sistemas en Oceanografía, Climatología y Ciencias Medio-Ambientales: Aspectos Mastemáticos y Numéricos. Imagraf, Málaga, pp. 89−102 (in Spanish).

Criado-Aldeanueva, F., García-Lafuente, J., Vargas, J.M., del Río, J., Vázquez, A., Reul, A., Sánchez, A., 2006. Distribution and circulation of water masses in the Gulf of Cádiz from in situ observations. Deep Sea Research Part II: Topical Studies in Oceanography 53, 1144−1160.

Dick, S., Schonfeld, W., 1996. Water transport and mixing in the North Frisian Wadden Sea. Results of numerical investigations. German Journal of Hydrography 48, 27−48.

Duursma, E.K., Carroll, J., 1996. Environmental Compartments. Springer, Berlin.

Echevarría, F., García-Lafuente, J., Bruno, M., Gorsky, G., Goutx, M., González, N., García, C.M., Gómez, F., Vargas, J.M., Picheral, M., Striby, L., Varela, M., Alonso, J.J., Reul, A., Cozar, A., Prieto, L., Sarhan, T., Plaza, F., Jiménez-Gómez, F., 2002. Physical−biological coupling in the Strait of Gibraltar. Deep Sea Research Part II: Topical Studies in Oceanography 49, 4115−4130.

Elbaz-Poulichet, F., Morley, N.H., Beckers, J.M., Nomerange, P., 2001. Metal fluxes through the Strait of Gibraltar: the influence of the Odiel and Tinto Rivers (SW Spain). Marine Chemistry 73, 193−213.

Fabres, J., Calafat, A., Sanchez-Vidal, A., Canals, M., Heussner, S., 2002. Composition and spatio-temporal variability of particle fluxes in the western Alborán gyre, Mediterranean Sea. Journal of Marine Systems 33−34, 431−456.

Farmer, D.M., Armi, L., 1988. The flow of Atlantic water through the Strait of Gibraltar. The flow of Mediterranean water through the Strait of Gibraltar. Progress in Oceanography 21, 1−105.

Freitas, P.S., Abrantes, F., 2002. Suspended particulate matter in the Mediterranean water at the Gulf of cadiz and off the southwest coast of the Iberian Peninsula. Deep Sea Research Part II: Topical Studies in Oceanography 49, 4245−4261.

Gascard, J.C., Richez, C., 1985. Water masses and circulation in the western Alborán Sea and in the Straits of Gibraltar. Progress in Oceanography 15, 157−216.

Gascó, C., Antón, M.P., Delfanti, R., González, A.M., Meral, J., Pappuci, C., 2002a. Variation of the activity concentrations and fluxes of natural (^{210}Po, ^{210}Pb) and anthropogenic (^{239,240}Pu, ^{137}Cs) radionuclides in the Strait of Gibraltar (Spain). Journal of Environmental Radioactivity 62, 241−262.

Gascó, C., Antón, M.P., Pozuelo, M., Meral, J., González, J.M., Papucci, C., Delfanti, R., 2002b. Distributions of Pu, Am and Cs in margin sediments from the western Mediterranean (Spanish coast). Journal of Environmental Radioactivity 59, 75−89.

Gómez, F., 2003. The role of exchanges through the Strait of Gibraltar on the budget of elements in the western Mediterranean Sea: consequences of human-induced modifications. Marine Pollution Bulletin 46, 685−694.

Greze, V.N., Kovalev, A.V., Baldina, E.P., Bileva, O.K., Shmeleva, A.A., 1985. Zooplankton transfer through the Strait of Gibraltar and peculiarities of its taxonomic composition and distribution in adjacent areas. Investigaciones Pesqueras 49, 3−13.

Heburn, G.W., La Violette, P., 1990. Variations in the structure of the anticyclonic gyres found in the Alborán Sea. Journal of Geophysical Research 95 (C2), 1599−1613.

Hirose, K., Igarashi, Y., Aoyama, M., Kim, C.K., Kim, C.S., Chang, B.W., 2003. Recent trends of plutonium fallout observed in Japan: plutonium as a proxy for desertification. Journal of Environmental Monitoring 5, 302−307.

IAEA, 2004. Sediment distribution coefficients and concentration factors for biota in the marine environment. Technical reports series 422, Vienna.

Ivanovich, M., Harmon, R.S., 1992. Uranium-series Disequilibrium: Applications to Earth, Marine and Environmental Sciences. Clarendon Press, Oxford.

Izquierdo, A., Tejedor, L., Sein, D.V., Backhaus, J.O., Brandt, P., Rubino, A., Kagan, B.A., 2001. Control variability and internal bore evolution in the Strait of Gibraltar: a 2D two-layer model study. Estuarine, Coastal and Shelf Science 53, 637−651.

Kowalick, Z., Murty, T.S., 1993. Numerical Modelling of Ocean Dynamics. World Scientific, Singapore.

Lacombe, H., Richez, C., 1982. The regime of the Strait of Gibraltar. In: Nihoul, J.C.J. (Ed.), Hydrodynamics of Semi-enclosed Seas. Elsevier, Amsterdam, pp. 13−73.

León-Vintró, L., Mitchell, P.I., Condren, O.M., Downes, A.B., Papucci, C., Delfanti, R., 1999. Vertical and horizontal fluxes of plutonium and americium in the western Mediterranean and the Strait of Gibraltar. The Science of the Total Environment 237/238, 77−91.

Liquete, C., Arnau, P., Canals, M., Colas, S., 2005. Mediterranean river systems of Andalusia, southern Spain, and associated deltas: a source to sink approach. Marine Geology 222/223, 471−495.

Liu, W.C., Hsu, M.H., Kuo, A.Y., 2002a. Modelling of hydrodynamics and cohesive sediment transport in Tanshui River estuarine system, Taiwan. Marine Pollution Bulletin 44, 1076−1088.

Liu, J.T., Chao, S., Hsu, R.T., 2002b. Numerical modeling study of sediment dispersal by a river plume. Continental Shelf Research 22, 1745−1773.

Lumborg, U., Windelin, A., 2003. Hydrography and cohesive sediment modelling: application to the Romo Dyb tidal area. Journal of Marine Systems 38, 287−303.

Mañanes, R., Bruno, M., Alonso, J., Fraguela, B., Tejedor, L., 1998. Non-linear interaction between tidal and subinertial barotropic flows in the Strait of Gibraltar. Oceanologica Acta 21, 33−46.

Masqué, P., Fabres, J., Canals, M., Sanchez-Cabeza, J.A., Sanchez-Vidal, A., Cacho, I., Calafat, A.M., Bruach, J.M., 2003. Accumulation rates of major consituents of hemipelagic sediments in the deep Alborán Sea: a centennial perspective of sedimentary dynamics. Marine Geology 193, 207−233.

Monte, L., Periáñez, R., Kivva, S., Laptev, G., Angeli, G., Barros, H., Zheleznyak, M., 2006. Assessment of state-of-the-art models for predicting the remobilisation of radionuclides following the flooding of heavily contaminated areas: the case of the Pripyat River floodplain. Journal of Environmental Radioactivity 88, 267−288.

Nyffeler, U.P., Li, Y.H., Santschi, P.H., 1984. A kinetic approach to describe trace element distribution between particles and solution in natural aquatic systems. Geochimica et Cosmochimica Acta 48, 1513−1522.

Parrilla, G., Kinder, T.H., Preller, R.H., 1986. Deep and intermediate Mediterranean water in the western Alborán Sea. Deep Sea Research 33, 55−88.

Periáñez, R., 1999. Three dimensional modelling of the tidal dispersion of non conservative radionuclides in the marine environment. Application to ^{239,240}Pu dispersion in the eastern Irish Sea. Journal of Marine Systems 22, 37−51.

Periáñez, R., 2000. Modelling the tidal dispersion of ^{137}Cs and ^{239,240}Pu in the English Channel. Journal of Environmental Radioactivity 49, 259−277.

Periáñez, R., 2002. The enhancement of ^{226}Ra in a tidal estuary due to the operation of fertilizer factories and redissolution from sediments: experimental results and a modelling study. Estuarine, Coastal and Shelf Science 54, 809−819.

Periáñez, R., 2003. Kinetic modelling of the dispersion of plutonium in the eastern Irish Sea: two approaches. Journal of Marine Systems 38, 259−275.

Periáñez, R., 2004a. A particle-tracking model for simulating pollutant dispersion in the Strait of Gibraltar. Marine Pollution Bulletin 49, 613−623.

Periáñez, R., 2004b. On the sensitivity of a marine dispersion model to parameters describing the transfers of radionuclides between the liquid and solid phases. Journal of Environmental Radioactivity 73, 101−115.

Periáñez, R., 2005a. Modelling the dispersion of radionuclides by a river plume. Application to the Rhone River. Continental Shelf Research 25, 1583−1603.
Periáñez, R., 2005b. Modelling the transport of suspended particulate matter by the Rhone River plume (France). Implications for pollutant dispersion. Environmental Pollution 133, 351−364.
Periáñez, R., 2005c. Modelling the Dispersion of Radionuclides in the Marine Environment. Springer-Verlag, Heidelberg.
Periáñez, R., 2006. Modelling surface radioactive spill dispersion in the Alborán Sea. Journal of Environmental Radioactivity 90, 48−67.
Periáñez, R., Martínez-Aguirre, A., 1997. U and Th concentrations in an estuary affected by phosphate fertilizer processing: experimental results and a modelling study. Journal of Environmental Radioactivity 35, 281−304.
Periáñez, R., Abril, J.M., García-León, M., 1996. Modelling the dispersion of non conservative radionuclides in tidal waters. Part 1: Conceptual and mathematical model. Journal of Environmental Radioactivity 31, 127−141.
Perkins, H., Kinder, T., La Violette, P., 1990. The Atlantic inflow in the western Alborán Sea. Journal of Physical Oceanography 20, 242−263.
Preller, R.H., 1986. A numerical model study of the Alborán Sea gyre. Progress in Oceanography 16, 113−146.
Pugh, D.T., 1987. Tides, Surges and Mean Sea Level. Wiley, Chichester.
Sánchez-Cabeza, J.A., Ortega, M., Merino, J., Masqué, P., 2002. Long-term box modelling of ^{137}Cs in the Mediterranean Sea. Journal of Marine Systems 33/34, 457−472.
Sannino, G., Bargagli, A., Artale, V., 2002. Numerical modelling of the mean exchange through the Strait of Gibraltar. Journal of Geophysical Research 107 (C8), 3094−3118.
Sannino, G., Bargagli, A., Artale, V., 2004. Numerical modelling of semidiurnal tidal exchange through the Strait of Gibraltar. Journal of Geophysical Research 109, C05011.
Sarmiento, J.L., Herbert, T., Toggweiler, J.R., 1988. Mediterranean nutrient balance and episodes of anoxia. Global Biogeochemical Cycles 14, 669−681.
Tappin, A.D., Burton, J.D., Millward, G.E., Statham, P.J., 1997. A numerical transport model for predicting the distributions of Cd, Cu, Ni, Pb and Zn in the southern North Sea: the sensitivity of model results to the uncertainties in the magnitudes of metal inputs. Journal of Marine Systems 13, 173−204.
Tattersall, G.R., Elliott, A.J., Lynn, N.M., 2003. Suspended sediment concentrations in the Tamar estuary. Estuarine, Coastal and Shelf Science 57, 679−688.
Tejedor, L., Izquierdo, A., Kagan, B.A., Sein, D.V., 1999. Simulation of the semidiurnal tides in the Strait of Gibraltar. Journal of Geophysical Research 104, 13541−13557.
Tsimplis, M.N., Bryden, H.L., 2000. Estimations of the transports through the Strait of Gibraltar. Deep Sea Research 47, 2219−2242.
Tsimplis, M.N., Proctor, R., Flather, R.A., 1995. A two dimensional tidal model for the Mediterranean Sea. Journal of Geophysical Research 100, 16223−16239.
Van Geen, A., Boyle, E., 1990. Variability of trace-metal fluxes through the Strait of Gibraltar. Palaeogeography, Palaeoclimatology, Palaeoecology 89, 65−79.
Vargas-Yáñez, M., Plaza, F., García-Lafuente, J., Sarhan, T., Vargas, J.M., Velez-Belchi, P., 2002. About the seasonal variability of the Alborán Sea circulation. Journal of Marine Systems 35, 229−248.
Vélez-Belchí, P., Vargas-Yáñez, M., Tintoré, J., 2005. Observation of a western Alborán gyre migration event. Progress in Oceanography 66, 190−210.
Vested, H.J., Baretta, J.W., Ekebjærg, L.C., Labrosse, A., 1996. Coupling of hydrodynamical transport and ecological models for 2D horizontal flow. Journal of Marine Systems 8, 255−267.
Werner, F.E., Cantos-Figueroa, A., Parrilla, G., 1988. A sensitivity study of reduced-gravity flows with applications to the Alborán Sea. Journal of Physical Oceanography 18, 373−383.